



PUBLICATION

MUSTANG

A MULTIPLE Space and Time scale Approach for the quaNTification of deep saline formations for CO₂ storaGe

Project Number: 227286

AUTHORS: G. Srinivasan, D.M. Tartakovsky, M. Dentz, H. Viswanathan, B. Berkowitz, B.A. Robinson

TITLE: Random walk particle tracking simulations of non-Fickian transport in heterogeneous media

The research leading to these results has received funding from the European Community's Seventh Framework Programme [FP7/2007/2013) under grant agreement n° [227286]

Status	AUTHOR VERSION
Date	2010
Publisher	Science Direct
Reference	Journal of Computational Physics, Vol. 229: 11, pp. 4304–4314, 2010

Random Walk Particle Tracking Simulations of Non-Fickian Transport in Heterogeneous Media

G. Srinivasan^a, D. M. Tartakovsky^b, M. Dentz^c, H. Viswanathan^d, B. Berkowitz^e, B. A. Robinson^d

^a*Theoretical Division, Los Alamos National Laboratory, Los Alamos, NM 87545, USA.*

^b*Department of Mechanical and Aerospace Engineering, University of California, San Diego, 9500 Gilman Drive, Mail Code 0411, La Jolla, CA 92093, USA*

^c*Institute of Environmental Assessment and Water Research (IDÆA-CSIC), Barcelona, Spain*

^d*Earth and Environmental Sciences Division, Los Alamos National Laboratory, Los Alamos, New Mexico, USA*

^e*Department of Environmental Sciences and Energy Research, Weizmann Institute of Science, Rehovot, Israel*

Abstract

Derivations of continuum nonlocal models of non-Fickian (anomalous) transport require assumptions that might limit their applicability. We present a particle-based algorithm, which obviates the need for many of these assumptions by allowing the stochastic processes representing the spatial and temporal random increments to be correlated in space and time, stationary or non-stationary, and to have arbitrary distributions. The approach treats a particle trajectory as a subordinated stochastic process that is described by a set of Langevin equations, which represent a continuous time random walk (CTRW). A convolution-based particle tracking (CBPT) is used to increase the computational efficiency and accuracy of these particle-based simulations. The combined CTRW-CBPT approach enables one to convert any particle-tracking legacy code into a simulator capable of handling non-Fickian transport.

Keywords: random walk, particle tracking, anomalous transport

Email addresses: gowri@lanl.gov (G. Srinivasan), dmt@ucsd.edu (D. M. Tartakovsky), marco.dentz@idaea.csic.es (M. Dentz)

1. Introduction

Many physical, biological, and biochemical phenomena [e.g., 1, 2, 3, 4] involve a combination of three passive transport mechanisms: advection, molecular diffusion, and hydrodynamic dispersion. Standard mathematical descriptions of such phenomena rely on an advection-dispersion equation (ADE),

$$\frac{\partial c}{\partial t} = \nabla \cdot (\mathbf{D}\nabla c) - \nabla \cdot (\mathbf{v}c), \quad (1)$$

where c is the volumetric concentration of a substance (e.g., solute), \mathbf{v} is the (macroscopic) advection velocity, and $\mathbf{D} = D_m\mathbf{I} + \mathbf{D}_d$ is the dispersion coefficient tensor defined as the sum of the molecular diffusion coefficient D_m (\mathbf{I} being the unit tensor) and the dispersivity tensor $\mathbf{D}_d = \mathbf{D}_d(\mathbf{v})$. Although the ADE proved to be indispensable in describing many transport processes, it has a number of drawbacks and limitations that are both computational and conceptual in nature.

Numerical solutions of the ADE (1) introduce “numerical dispersion”, which manifests itself in excessive smearing of concentration profiles at large Péclet numbers. This problem is exacerbated by high degrees of anisotropy that often characterize hydrodynamic dispersion. For example, transport in natural porous media typically exhibit longitudinal dispersivities that are two orders of magnitude higher than their transverse counterparts [5]. Numerical dispersion can be controlled by employing Eulerian-Lagrangian [6, 7] and other [8] algorithms, many of which are computationally expensive.

A more fundamental shortcoming of the macroscale ADE (1) is its inability to capture anomalous or non-Fickian transport behavior, which is often observed in heterogeneous environments [9, 10, 11, 12, 13, 14]. This failure can be attributed to subgrid-scale heterogeneity that is not resolved at the support scale on which the parameters of the ADE are defined. If it is possible to resolve the heterogeneity structure on all scales, the corresponding ADE reflects the related anomalous transport behavior [e.g., 15]. This is not very realistic for many practical applications.

This shortcoming of the macroscale ADE can be effectively overcome by replacing the ADE (1) with its counterparts that are *nonlocal* in space and/or time. Derivations of nonlocal transport equations rely on a number of assumptions. For example, stochastic derivations of nonlocal mean transport equations often require velocity fluctuations to be either small [16] or Gaussian [17]; and standard derivations of both fractional ADEs (fADEs) [18, 19]

31 and effective equations of continuous time random walk (CTRW) models
32 [20, 21, 22, 23, 24] are based on the assumption that subgrid scale fluctu-
33 ations are space-time stationary. Particle-based simulations provide a com-
34 putationally efficient framework for solving both local and nonlocal effective
35 transport equations. Particle-tracking algorithms (PTAs) are used routinely
36 to control numerical dispersion in solutions of the ADE (1) [25, 26, 27, 28, 29]
37 and, more recently, to solve nonlocal effective transport equations based on
38 CTRW [30, 31, 32, 33], fADE [34], and multirate mass transfer [35, 36]. Ad-
39 vantages and disadvantages of using PTAs to solve the ADE (1), e.g., the
40 challenges posed by local mass conservation and a large number of particles
41 that are needed to obtain smooth concentration profiles, are discussed in [37].
42 Solving nonlocal effective models with PTAs does not relax the assumptions
43 that are required for their derivation.

44 We introduce a particle-based approach for modeling non-Fickian (anoma-
45 lous) transport in heterogeneous environments that requires no assumption
46 about statistical properties of the model parameters. To increase the compu-
47 tational efficiency and accuracy of the particle-based simulations, we employ
48 the convolution-based particle tracking (CBPT) method [38]. An added ben-
49 efit of the proposed approach lies in its ability to convert any existing (legacy)
50 particle-tracking code into a simulator capable of handling non-Fickian be-
51 havior.

52 Particle tracking algorithms for solving the ADE (1) utilize its equiva-
53 lence to the Langevin equation, which describes a solute particle’s trajectory
54 as a stochastic process [39]. Introducing a randomized time step into this
55 process yields a new “subordinated” stochastic process that is capable of cap-
56 turing anomalous transport behavior [e.g., 40]. This subordinated process is
57 described by a set of Langevin equations, which represent a CTRW [e.g., 41].
58 In this paper, we adopt a general Langevin approach that imposes no sta-
59 tistical restrictions on the stochastic processes representing the spatial and
60 temporal random increments. Each of these two processes can be correlated,
61 non-stationary, and cross-correlated with the other, as well as have arbitrary
62 distributions.

63 Employing this subordination strategy, we obtain a simple method to
64 convert any random walk particle-tracking simulator into a continuous time
65 random walk simulator. This enables us to achieve two computational advan-
66 tages. First, the proposed approach is non-intrusive in that it allows one to
67 use any existing particle tracking simulator for modeling non-Fickian behav-
68 ior. Second, the proposed approach is applicable to heterogeneous and non-

69 stationary fields, whereas standard continuum formulations of non-Fickian
70 transport require stationarity and statistical homogeneity. For stationary and
71 uncorrelated random increments the well known partial differential equation
72 (PDE) formulations of CTRW in terms of generalized Fokker-Planck equa-
73 tions [23] can be obtained by a generalized Kramers-Moyal expansion [e.g.,
74 42]. The two components of the proposed approach, CBPT and CTRW, are
75 described in Sections 2 and 3, respectively. The computational algorithm
76 is presented in Section 3.1. Section 4.1 contains a computational example
77 that can be solved analytically and, hence, is used to analyze the accuracy
78 and robustness of our algorithm. In Section 4.2, we apply the algorithm to
79 model non-Fickian transport in two separate three-dimensional macroscopi-
80 cally heterogeneous porous media; the simulation results are contrasted with
81 those obtained by solving the classical ADE (1). Section 5 provides a brief
82 summary of the results and conclusions.

83 2. Convolution-Based Particle Tracking (CBPT)

A standard random walk particle tracking [e.g., 28] solves the ADE (1) based on the equivalence of the ADE and the following Langevin equation [e.g., 39]

$$\mathbf{X}(t + \Delta t) = \mathbf{X}(t) + \mathbf{A}[\mathbf{X}(t)]\Delta t + \mathbf{B}[\mathbf{X}(t)] \cdot \boldsymbol{\xi} \sqrt{\Delta t}. \quad (2)$$

Here $\mathbf{X}(t) = [X_1(t), X_2(t), X_3(t)]^T$ is the random particle location at time t , $\boldsymbol{\xi} = [\xi_1, \xi_2, \xi_3]^T$ is Gaussian white noise with zero mean and unit variance,

$$\langle \xi_i \rangle = 0, \quad \langle \xi_i \xi_j \rangle = \delta_{ij} \quad (3)$$

The drift vector \mathbf{A} and the second-order tensor \mathbf{B} are related to the coefficients in (1) by [e.g., 25]

$$\mathbf{A} = \mathbf{v} + \nabla \mathbf{D}, \quad \mathbf{B}\mathbf{B}^T = 2\mathbf{D}. \quad (4)$$

84 The particle's initial position, or its label, is given by $\mathbf{X}(t = 0) = \mathbf{x}_0$.

The CBPT [38] accelerates the convergence of the particle-tracking algorithm (2)–(4), i.e., requires fewer particles, by taking advantage of the linearity of the ADE (1). Let $g(\mathbf{x}, t - \tau | \mathbf{x}_0)$ denote the Green's function for (1), which is defined as a solution of the adjoint equation

$$\frac{\partial g}{\partial \tau} = \nabla \cdot (\mathbf{D} \nabla g) + \mathbf{v} \cdot \nabla g, \quad (5)$$

subject to the initial condition $g(\mathbf{x}, \tau = t | \mathbf{x}_0) = \delta(\mathbf{x} - \mathbf{x}_0)$ and appropriate homogeneous boundary conditions. The Green's function $g(\mathbf{x}, t | \mathbf{x}_0)$ can be expressed in terms of particle trajectories as [e.g., 39]

$$g(\mathbf{x}, t | \mathbf{x}_0) = \langle \delta[\mathbf{x} - \mathbf{X}(t)] \rangle |_{\mathbf{x}(0)=\mathbf{x}_0}, \quad (6)$$

85 where the angular bracket denotes the ensemble average over the random
 86 vector $\boldsymbol{\xi}$. We use the particle tracking algorithm (2) and (6) to compute the
 87 Green's function $g(\mathbf{x}, t - \tau | \mathbf{x}_0)$.

Concentration $c(\mathbf{x}, t)$ resulting from spatially and/or temporally distributed sources $\dot{m}(\mathbf{x}', t')$ can now be computed as

$$c(\mathbf{x}, t) = \int_0^t \int_{\Omega} \dot{m}(\mathbf{x}_0, \tau) g(\mathbf{x}, t - \tau | \mathbf{x}_0) d\mathbf{x}_0 d\tau, \quad (7)$$

88 where Ω is the computational domain. The accuracy and computational
 89 efficiency of the CBPT (2), (6), and (7) are analyzed in detail in [38]. For
 90 the computational example described in Section 4.1, the performance of the
 91 CBPT algorithm is demonstrated in Table 1.

Number of particles	Duration of mass injection (Years)	CBPT method, ϵ	Conventional method, ϵ
10^5	1000	0.0154	0.433
10^5	100	0.0301	0.177
10^5	10	0.0698	0.0925
10^5	1	0.122	0.119

Table 1: Performance metrics for the CBPT and conventional particle-tracking methods.

The performance metric ϵ in Table 1 is defined as

$$\epsilon = \frac{1}{N} \sqrt{\sum_{i=1}^N \left[\frac{c_{\text{ex}}(\mathbf{x}_i) - c_{\text{nu}}(\mathbf{x}_i)}{c_{\text{ex}}(\mathbf{x}_i)} \right]^2}, \quad (8)$$

92 where c_{ex} is the “exact” concentration computed with an analytical solution,
 93 c_{nu} is the concentration predicted by a numerical method, i.e., by either the
 94 CBPT or the conventional particle tracking method, and N is the number
 95 of observations. It can be seen that the CBPT method is always at least

96 as accurate as the conventional particle tracking methods and needs fewer
 97 particles to achieve the same accuracy in most cases, especially for larger
 98 solute injection times. The concentration as a function of distance from the
 center of the plume is plotted in Figure 1.

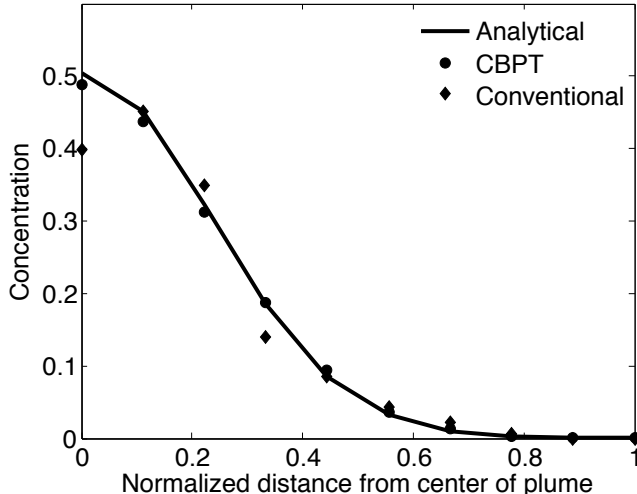


Figure 1: Concentration $c(x_1, t)$ at time $t = 1000$ y predicted with the analytical solution, the conventional particle-tracking method, and the CBPT.

99

100 3. Continuous Time Random Walk (CTRW)

The random walk model (2)–(4) treats the time step $\tau \equiv \Delta t$ as deterministic and the transition-length vector $\boldsymbol{\xi}$ as random, which results in Fickian dispersion. Let us introduce the randomized or operational time $s(t)$ [e.g., 40] defined as a “renewal process” [e.g., 43, 44] that is conjugate to

$$\frac{dt(s)}{ds} = \tau(s), \quad (9)$$

where $\tau(s)$ is a random process to be specified below. The random trajectory becomes an implicit function of time, $\mathbf{X}[s(t)]$. Thus, we obtain the subordinated system of Langevin equations [e.g., 41]

$$\mathbf{X}(s_n + \Delta s) = \mathbf{X}(s_n) + \mathbf{A}[\mathbf{X}(s_n)]\Delta s + \mathbf{B}[\mathbf{X}(s_n)] \cdot \boldsymbol{\xi}(s_n)\sqrt{\Delta s} \quad (10a)$$

$$t(s_n + \Delta s) = t(s_n) + \tau(s_n)\Delta s, \quad (10b)$$

101 where \mathbf{A} and \mathbf{B} are defined in (4), Δs is the constant increment of the dis-
 102 cretized operational time $s_n = n\Delta s$. In general, the random series $\{\boldsymbol{\xi}(s_n)\}$
 103 and $\{\tau(s_n)\}$ can be correlated or uncorrelated, stationary or nonstationary,
 104 and have arbitrary distributions. As pointed out in the Introduction, this
 105 formulation is quite general and provides an alternative to PDE formula-
 106 tions of CTRW that assume statistical stationarity and independence of the
 107 stochastic processes $\{\boldsymbol{\xi}(s)\}$ and $\{\tau(s)\}$. Furthermore, note that PDE formula-
 108 tions in terms of non-local Fokker-Planck equations typically rely on the
 109 truncation of a Kramers-Moyal expansion after the second-order term [e.g.,
 110 39, 21]. The validity of this truncation in the CTRW framework for a Gaus-
 111 sian white noise $\{\boldsymbol{\xi}(s)\}$ has been demonstrated in [30] by using random walk
 112 particle tracking simulations.

To facilitate the comparison with the existing CTRW literature, in the
 following we take each of the processes $\{\boldsymbol{\xi}(s)\}$ and $\{\tau(s)\}$ to be uncorrelated
 and characterized by the joint probability density

$$\mathcal{P} [\{\boldsymbol{\xi}(s_n); \tau(s_n)\}_{n=1}^N] = \prod_{n=1}^N \psi[\boldsymbol{\xi}(s_n), \tau(s_n)], \quad (11)$$

113 where $\psi(\boldsymbol{\xi}, \tau)$ is the joint transition length and time distribution density.
 114 The principal of causality requires that the temporal random process satisfy
 115 the condition $t(s_{n+1}) \geq t(s_n)$, which implies that $\tau(s_n) \geq 0$. The system of
 116 Langevin equations (10) describes particle motion as a CTRW in a macro-
 117 scopically heterogeneous medium.

118 The choice of the probability density $\psi(\boldsymbol{\xi}, \tau)$ is crucial to simulating non-
 119 Fickian transport in (randomly) heterogeneous environments, which are char-
 120 acterized by evolving hierarchies of length scales.

121 Some approaches and criteria for computing or selecting $\psi(\boldsymbol{\xi}, \tau)$ can be
 122 found in [e.g., 45, 22]. Here we consider random walks that are mutually
 123 uncorrelated in space and time, so that the joint probability density $\psi(\boldsymbol{\xi}, \tau)$
 124 can be decoupled, i.e., $\psi(\boldsymbol{\xi}, \tau) = \psi_s(\boldsymbol{\xi})\psi_t(\tau)$.

Furthermore, in the following we assume that transition times on a deter-
 ministic time interval $[t_1, t_2]$ follow a truncated power-law distribution [e.g.,
 30, 46]

$$\psi_t(\tau) = \frac{r^\beta(1 + \tau/t_1)^{-1-\beta}}{t_1\Gamma(-\beta, r)} e^{-r-\tau/t_2}, \quad r = \frac{t_1}{t_2}, \quad 0 \leq \beta \leq 2, \quad (12)$$

125 where $\Gamma(a, x)$ is the incomplete Gamma function. The median transit time is
 126 set equal to the increment of the operational time, $t_1 = \Delta s$. For times $\tau > t_2$,
 127 $\psi_t(\tau)$ decreases exponentially fast. The transport behavior is anomalous in
 128 the transition regime $t_1 \leq t \leq t_2$ and becomes Fickian for large times $t > t_2$.

129 3.1. Simulation Algorithm

The Green's function $\bar{g}(\mathbf{x}, t|\mathbf{x}_0)$ is given in terms of the particle trajectories of the CTRW (10) by

$$\bar{g}(\mathbf{x}, t|\mathbf{x}_0) = \langle \delta\{\mathbf{x} - \mathbf{X}[s(t)]\} \rangle_{\mathbf{x}(0)=\mathbf{x}_0}, \quad (13)$$

where the angular brackets denote the average over the spatial and temporal random processes $\{\boldsymbol{\xi}(s)\}$ and $\{\tau(s)\}$. Note that the particle trajectory here is an implicit function of time, $\mathbf{X}(t) \equiv \mathbf{X}[s(t)]$. Expression (13) can be written as

$$\bar{g}(\mathbf{x}, t|\mathbf{x}_0) = \int_0^\infty ds \langle \delta[\mathbf{x} - \mathbf{X}(s)] \delta[s - s(t)] \rangle_{\mathbf{x}(0)=\mathbf{x}_0}. \quad (14)$$

We discretize the operational time s according to $s_n = n\Delta s$ and $s(t) = N_t\Delta s$, where the discrete process N_t is defined by

$$N_t = \min(n|t(s_{n+1}) > t) \quad (15)$$

Thus, we obtain for $\bar{g}(\mathbf{x}, t|\mathbf{x}_0)$ the expression [e.g., 47]

$$\bar{g}(\mathbf{x}, t|\mathbf{x}_0) = \sum_{n=0}^\infty \langle \delta[\mathbf{x} - \mathbf{X}(s_n)] \delta_{n, N_t} \rangle_{\mathbf{x}(0)=\mathbf{x}_0} = \langle \delta[\mathbf{x} - \mathbf{X}(s_{N_t})] \rangle_{\mathbf{x}(0)=\mathbf{x}_0}. \quad (16)$$

130 This relation provides a straightforward recipe on how to obtain $\bar{g}(\mathbf{x}, t)$.
 131 The solution for the concentration profile for a general source distribution
 132 then is calculated by the convolution of the source term with \bar{g} as expressed
 133 by (7). The corresponding algorithm combines the CBPT and CTRW ap-
 134 proaches and consists of the following steps.

- 135 1. Starting from a point source at \mathbf{x}_0 at time $t = 0$, the spatio-temporal
 136 particle trajectories are tracked according to (10). After N_t steps, that
 137 is, when the simulation time t is between t_N and t_{N+1} , $t_N \leq t < t_{N+1}$,
 138 the position \mathbf{x}_N is recorded. The Green's function \bar{g} is determined by
 139 sampling the particle positions in space according to (16).

140 2. Finally, the anomalous concentration profile is obtained by convolving
141 \bar{g} with the source term.

142 This algorithm renders itself to straightforward integration into most ex-
143 isting legacy codes, as we do below for the DOE-certified code Finite Element
144 Heat and Mass Transfer Code (FEHM) [48]. Next, we apply this code to three
145 computational examples of increasing difficulty. The example in Section 4.1 is
146 used to demonstrate the accuracy and computational efficiency of the CBPT.
147 Section 4.2 provides two examples of the use of the CBPT-CTRW to model
148 anomalous transport in realistic three-dimensional geological settings.

149 *3.2. Integration Into Legacy Codes*

150 FEHM is a multiphase, multidimensional reservoir simulator. In order to
151 calculate the velocity field, FEHM simulations may include numerous cou-
152 pled processes including thermo-hydro-chemical-mechanical (THCM). These
153 coupled processes are often important for studies of carbon sequestration,
154 nuclear waste disposal, and hazardous waste disposal. It currently lacks the
155 capability of handling anomalous transport. It relies on a three-dimensional
156 node based particle tracking method that takes advantage of the fluxes at
157 nodes being given by the flow solution, and can be used easily with un-
158 structured grids etc, without having to use interpolation schemes. By using
159 the velocity field from the flow simulation, the particle tracking algorithm
160 takes advantage of the complex velocity field calculated by the flow simula-
161 tion that often depends on the numerous coupled processes mentioned above.
162 The proposed algorithm can be used with any node based particle tracking
163 technique.

164 **4. Transport in Macroscopically Homogeneous and Heterogeneous** 165 **Media**

166 In this section, we apply the random walk algorithm presented above
167 to transport in macroscopically homogeneous and heterogeneous media. The
168 code is validated against known solutions for instantaneous sources in macro-
169 scopically homogeneous media [30] and applied to solute transport evolving
170 from continuous solute injections in macroscopically homogeneous and het-
171 erogeneous media.

172 *4.1. Macroscopically Homogeneous Medium*

173 Consider solute transport in a three-dimensional macroscopically homo-
 174 geneous porous medium $\Omega = [0, \infty] \times [0, L_2] \times [0, L_3]$. Flow velocity \mathbf{v} is taken
 175 to be constant and aligned with the x_1 coordinate axis, $\mathbf{v} = [v, 0, 0]^T$ with
 176 $v = 34.2$ m/y. The longitudinal dispersivity is set to $\alpha_L = 500$ m, the corre-
 177 sponding longitudinal dispersion coefficient is $D_L = \alpha_L v$, and the transverse
 178 horizontal and vertical dispersion are neglected, $D_T = 0$. Constant head
 179 boundaries are prescribed at the inlet and outlet, with a difference in head
 180 of 0.377 MPa. The porosity and permeability are constant throughout the
 181 medium with values of $\omega = 0.03361$ and $k = 10^{-12}$ m², respectively. The pa-
 182 rameters are chosen such that the resulting flow translates into a mean travel
 183 time of 500 y to reach the outlet. Regardless of the transport model used,
 184 this parameter choice renders transport one-dimensional, $c(\mathbf{x}, t) = c(x_1, t)$.

The initial concentration is set to $c(x_1, t = 0) = 0$. The boundary condi-
 tion at $x_1 = 0$ is more conveniently expressed in terms of the flux-averaged
 concentration [49]

$$c_f(x_1, t) = v^{-1} \int_0^{x_1} \frac{\partial c(x'_1, t)}{\partial t} dx'_1. \quad (17)$$

At the inlet $x_1 = 0$, $c_f(x_1, t)$ is given by

$$c_f(x_1 = 0, t) = j(t)/v, \quad (18)$$

185 where $j(t)$ is the boundary flux. The concentration and concentration flux
 186 are zero at the boundary at infinity. We study transport in terms of spatial
 187 profiles, that is snapshots of $c(x_1, t)$ and breakthrough curves at a given
 188 distance. The latter are equivalent to first passage time distributions at a
 189 control plane. They are obtained from the flux-averaged concentration. In
 190 these simulations, the domain Ω is discretized with grid spacings $\Delta x_1 = 400$
 191 m.

192 *4.1.1. Validation of the Simulation Algorithm*

Here, we validate the simulation algorithm against known solutions for
 the flux-averaged concentration $c_f(x_1, t)$ with a constant, continuous injec-
 tion at the inlet, that is, $j(t) = v$ at $x_1 = 0$ using a total of 10^4 particles. For
 stationary and uncorrelated random increments, the CTRW (10) admits a

PDE representation in terms of a temporally non-local Fokker-Planck equation [e.g., 23, 21, 30]. Dentz et al. [30] studied resident and flux-averaged concentrations for anomalous transport in a macroscopically homogeneous medium using random walk simulations as well as Laplace space solutions of the equivalent generalized Fokker-Planck equations. For the above specified boundary and initial conditions, they provide for the Laplace transform of the flux-averaged concentration the following expression

$$\tilde{c}_f(\lambda, x_1) = \exp \left[-\frac{vx_1}{2D_L} \left(\sqrt{1 + 4\frac{\lambda D_L}{\tilde{M}v^2}} - 1 \right) \right]. \quad (19a)$$

Here the tilde indicates Laplace transforms, λ is the Laplace variable, \tilde{M} is the Laplace transform of the memory function defined as

$$\tilde{M}(\lambda) = \frac{t_1 \lambda \tilde{\psi}_t(\lambda)}{1 - \tilde{\psi}_t(\lambda)} \quad (19b)$$

193 and $\tilde{\psi}_t(\lambda)$ is the Laplace transform of $\psi_t(t)$ in (12). The Laplace transform
 194 of the concentration $c(x_1, t)$ given by a solution of the ADE (1) is recovered
 195 from (19a) by setting $\tilde{M} \equiv 1$.

196 The analytical solution (19) is used to analyze the convergence of the
 197 CBPT and to validate the particle tracking implementation of the CTRW
 198 (10a)–(12) (the simulation algorithm in Section 3.1). Figure 2 compares the
 199 accuracy of the CBPT for both classical (Fig 2a) and anomalous (Fig 2b)
 200 transport. In the latter case, the CBPT is an integral part of the CBPT-
 201 CTRW algorithm described in Section 3.1. In both cases, the Laplace trans-
 202 form (19) of concentration for the analytical solution is inverted with the
 203 algorithm of de Hoog [50].

204 The breakthrough is computed at a distance of $x = 15.2$ km over a total
 205 time of 3000 y. The results from both analytical and numerical (the CBPT-
 206 CTRW algorithm) simulations are plotted in Figure 2 for the ADE and $\beta =$
 207 1.25. The analytical solutions shown as circles and the numerical solutions
 208 represented by solid lines are in excellent agreement with each other. Such
 209 continuous injection scenarios are of practical importance for the modeling
 210 of contamination events in industrial plants, where contaminants can leak
 211 into the subsurface over many years, underground nuclear waste storage, as
 212 well as for the modeling of heat plumes in the subsurface that are generated
 213 by heat exchangers.

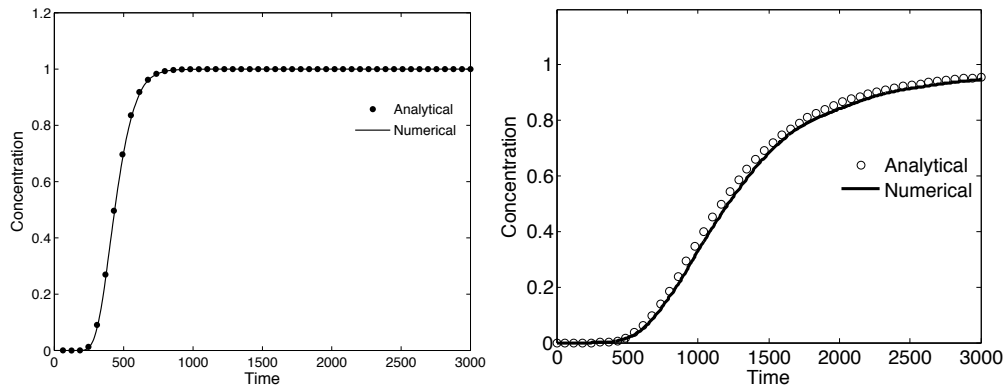


Figure 2: The breakthrough curves at $x_1 = 15.2$ km predicted with (a) the classical and (b) anomalous ($\beta = 1.25$) models of transport.

214 *4.1.2. Breakthrough Curves and Spatial Profiles*

215 An often neglected aspect of contaminant transport is the spatial nature
 216 of the plume across the entire field of study, since PTAs are mostly concerned
 217 with the breakthrough across a control plane. In this section, we present both
 218 breakthrough curves as well as the spatial concentration distribution for pulse
 219 injection $j(t) = v\delta(t)$ at the inlet $x_1 = 0$.

220 As in [30], we study the the effects on anomalous transport of the three
 221 key parameters in the CTRW model defined by the truncated power-law
 222 waiting time distribution (12): the median waiting time t_1 , the cut-off time
 223 t_2 after which transport becomes Fickian, and the exponent β .

224 Consequently, we set $t_1 = 4$ y and $t_2 = 10^4$ y, and focus on the effects
 225 of $0 \leq \beta \leq 2$. It has been shown [e.g., 22] that $\beta = 2$ asymptotically leads
 226 to the Fickian behavior as predicted with the ADE (1) and that deviations
 227 from the Fickian transport become stronger as β becomes smaller.

228 Figure 3 depicts the breakthrough curves resulting from the pulsed bound-
 229 ary condition, $c(0, t) \equiv 1$ for $t \leq 10^3$ y and $c(0, t) \equiv 0$ for $t > 10^3$ y. The
 230 breakthroughs computed with the particle tracking simulations of the classi-
 231 cal and anomalous transport are shown for several values of β .

232 In accordance with the theory, $\beta = 2$ gives rise to the classical transport
 233 behavior in terms of breakthrough times, peak concentrations, and Gaus-
 234 sianity of concentration profiles. As β decreases, breakthrough times become
 235 larger and concentration profiles exhibit progressively longer tails. The peak
 236 breakthrough values of concentration become progressively smaller, since the
 237 area under the breakthrough curves (i.e., total mass) is constant. The num-

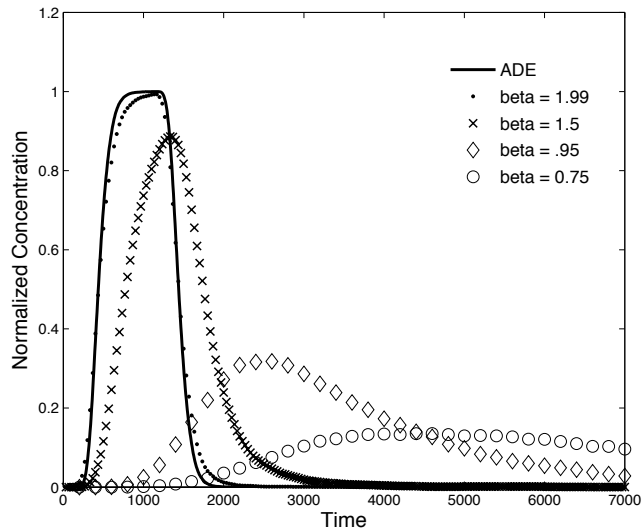


Figure 3: Breakthrough curves of concentration $c(x_1, t)$ at $x_1 = 15.2$ km for the pulsed input at the inlet $x_1 = 0$.

238 ber of particles that is required to represent breakthrough curves within a
 239 given tolerance level increases as β decreases and the deviation from the
 240 Gaussian behavior becomes more pronounced.

241 Figure 4 exhibits the temporal evolution of the concentration profiles for
 242 several values of β . The classical transport model (ADE or $\beta = 2$) exhibits
 243 no tailing and predicts that the solute occupies the entire computational
 244 domain by $t = 2000$ y. For $\beta = 1.99$, the tailing is very small and most of the
 245 mass has broken through by $t = 2000$ y and all of it by $t = 3000$ y. While
 246 $\beta = 1.5$ leads to a significant tailing, the arrival at the outlet starts to taper
 247 off by 2000 y. The concentration profiles corresponding to $\beta < 1$ indicate
 248 that mass is still breaking through at the end of the simulation time.

249 Figure 4 also reveals that the concentration at the inlet $x_1 = 0$ increases
 250 with decreasing β . This is because smaller values of β correspond to larger
 251 residence times in a boundary cell, resulting in a slower rate of transport
 252 across the medium and hence later arrival at the cross-section $x_1 = 15.2$ km.
 253 This is a mathematical representation of subscale mass transfer processes,
 254 such as diffusion into dead-end pores, which retard the solute migration.

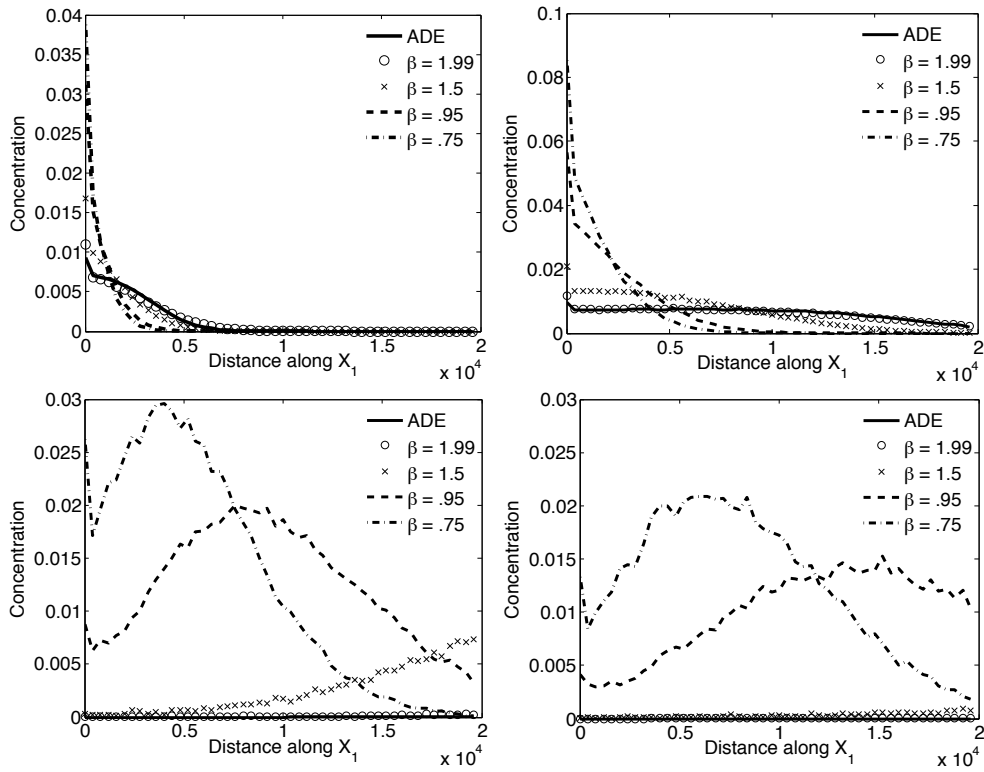


Figure 4: Concentration profiles $c(x,t)$ at (a) $t = 100$ y, (b) $t = 500$ y, (c) $t = 2000$ y, and (d) $t = 3000$ y for pulsed input at the inlet

255 *4.2. Macroscopically Heterogeneous Medium*

256 We use the CBPT-CTRW algorithm to simulate anomalous transport
257 in heterogeneous media using two examples presented here. We consider
258 in both examples, a three-dimensional heterogeneous porous medium $\Omega =$
259 $[0, L_1] \times [0, L_2] \times [0, L_3]$. The simulation results presented below correspond
260 to $L_1 = 20$ km, $L_2 = 9.6$ km and $L_3 = 5$ km.

261 In the first example, the model was divided into 4 equal zones in the
262 primary flow direction, spanning $5km$ each. The initial zone and final zone
263 have the same properties as the homogeneous media example of the previous
264 section. The second zone has a reduced porosity of $\omega = 0.01425$ and the
265 third zone a reduced permeability of $k = 10^{-13}$ m². The simulations below
266 correspond to $H_1 - H_2 = 0.377$ MPa. The rest of the boundaries are imper-
267 meable to flow. To solve the flow equation (20) with the finite element code
268 FEHM, the domain is discretized with a total of $51 \times 25 \times 101 = 128,775$
269 nodes in the x_1 , x_2 , and x_3 directions, respectively. The transport equations
270 were solved using 10^4 particles.

271 Lower porosities result in faster movement of particles through zone 2.
272 The overall flow is slower, as a result of the lower permeability across one
273 of the four zones, since the effective permeability is a harmonic mean of the
274 different permeability values. The breakthrough point for these simulations
275 was at $L_1 = 15.2km$. The simulation was performed for 3000 years and
276 tracer injected continuously for the entire length of the simulation. The
277 Breakthrough Curve (Fig 5) is shown for the ADE as well as for the case of
278 $\beta = 1.25$.

279 This example demonstrates the effects of large scale heterogeneity on
280 contaminant transport. Features such as high permeability faults or low
281 permeability clay lenses can be represented in this manner.

282 In the second example, we take a geostatistical approach for representing
283 heterogeneity. In the subsurface, permeability distributions often follow a
284 log-normal permeability distribution and are correlated. If large scale fea-
285 tures are not present or known, a log-normal permeability distribution is
286 often used simulate the structure of the permeability field. The mean, vari-
287 ance, and correlation length are quantities that can be obtained from field
288 measurements. These parameterse can then be used to generate synthetic
289 permeability fields. In the second case studied, in addition to the longitu-
290 dinal dispersion coefficient specified in Section 4.1, we define the transverse
291 dispersion coefficient as $D_T = \alpha_T |\mathbf{v}|$ where the transverse dispersivity is set

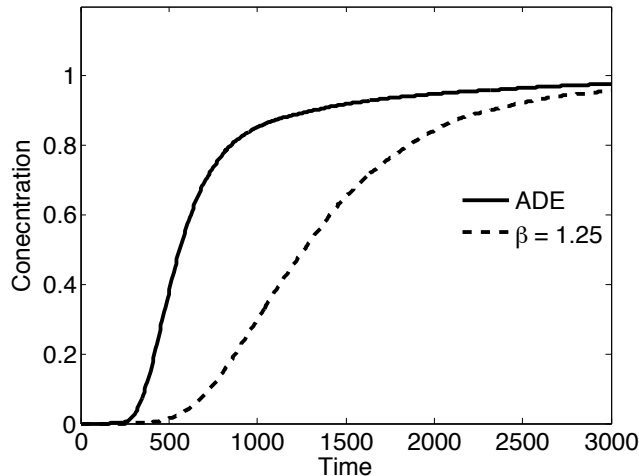


Figure 5: Comparison of the ADE and CTRW methods for flow through heterogeneous medium. Breakthrough curves of concentration $c(x_1, t)$ at $x_1 = 15.2$ km for continuous injection at the inlet $x_1 = 0$.

292 to $\alpha_T = 50$ m. We specify a pulse boundary condition at the inlet, inject-
 293 ing 10^4 particles uniformly over a 100 m distance at the top edge, $x_1 = 0$,
 294 $x_2 = L_2$.

295 The medium’s permeability $k(\mathbf{x})$ —the top subfigure in Figure 6—was
 296 constructed using a multiresolution random field generator based on the
 297 Karhunen-Loève decomposition [51]. It represents a realization of the sta-
 298 tistically homogeneous random field that has the mean $\bar{k} = 10^{-12}$ m², trans-
 299 formed variance $\sigma_{\ln k}^2 = 1$, and anisotropic exponential covariance function
 300 with correlation lengths 200 m, 200 m, and 100 m in the x_1 , x_2 and x_3 direc-
 301 tions, respectively. Tracer was injected for the first 1000 y of the simulation.

The medium’s heterogeneity causes spatial variability of the fluid velocity $\mathbf{v}(\mathbf{x})$. It is computed by rescaling the Darcy flux $\mathbf{q}(\mathbf{x})$ with the medium’s (constant) porosity ω , i.e., $\mathbf{v} = \mathbf{q}/\omega$. The Darcy flux is obtained as a solution of the steady-state flow equation,

$$\mathbf{q} = -\frac{kg}{\nu}\nabla h, \quad \nabla \cdot \mathbf{q} = 0, \quad (20)$$

302 where ν is the fluid’s kinematic viscosity, g is the gravitational constant
 303 and $h(\mathbf{x})$ is the hydraulic head. The flow is driven by the hydraulic head
 304 gradient resulting from boundary conditions $h(x_1 = 0, x_2, x_3) = H_1$ and

305 $h(x_1 = L_1, x_2, x_3) = H_2$. The boundary conditions and domain discretiza-
 306 tion for this example was the same as the previous heterogeneous medium
 307 example.

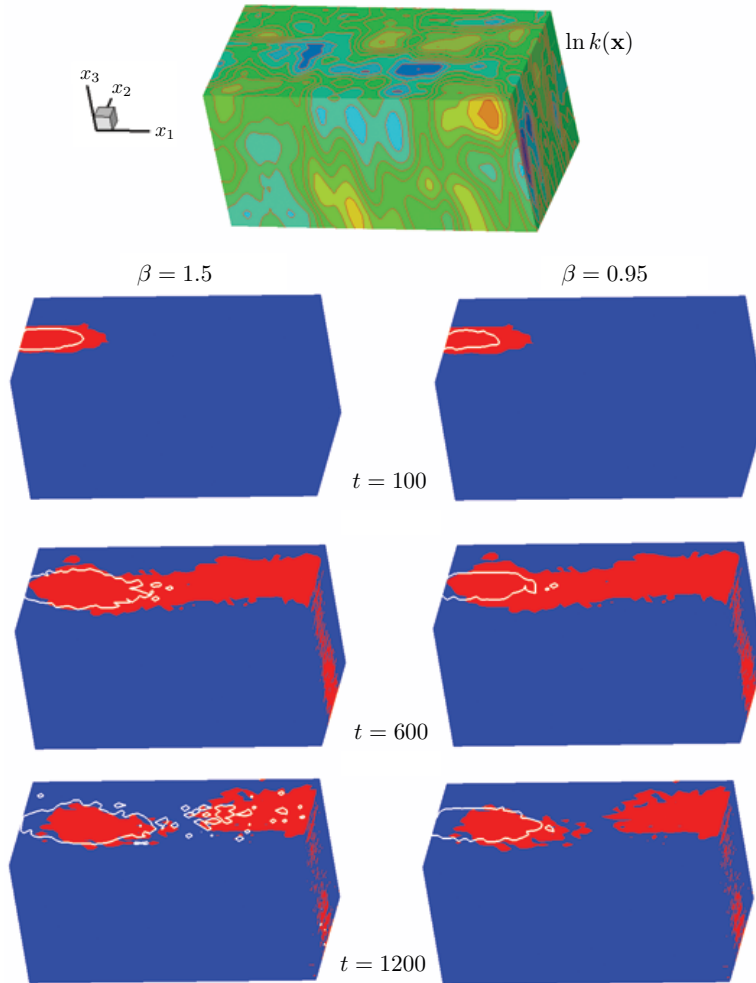


Figure 6: Comparison of the ADE and CTRW methods for flow through heterogeneous permeability field. The ADE plume is shown in red and the CTRW plume in white.

308 The results of these simulations are presented in Figure 6 for anomalous
 309 transport with $\beta = 1.5$ and $\beta = 0.95$, as well as for the ADE model of
 310 transport. Iso-surface plots of the model domain are shown at various times,
 311 100 y, 600 y and 1200 y. A normalized concentration of 0.0025 was chosen for
 312 the isoline with the ADE plume shown in red and the CBPT-CTRW shown

313 in white. Since the tracer is injected near the top surface of the domain, the
314 majority of the plumes travel along the top surface of the model domain. As
315 time progresses, the plumes appear to break apart into “islands” at the top
316 surface. The islands are due to the fact that there are low permeability zones
317 that cause the plume to leave the top surface later reappears due to high
318 permeability pathways. The CBPT-CTRW algorithm predicts significant
319 attenuation of the plume for both values of β . It resulted in lower peak
320 concentration and longer tail breakthrough curves than those resulting from
321 the ADE. Lower values of β lead to higher values of the inlet concentration
322 at later times, since they correspond to larger residence times in a cell. The
323 distance traveled by the plume also decreases as β decreases. Relative to
324 its counterpart predicted with the ADE, it spreads farther in the transverse
325 direction.

326 5. Conclusions

327 Advection-dispersion equations (ADEs) are routinely used to describe
328 transport phenomena in heterogeneous environments. Yet they often fail to
329 capture subgrid heterogeneities that lead to the so-called anomalous or non-
330 Fickian transport behavior, whose manifestations are early or late arrival
331 times, long tails of concentration profiles, etc.

332 We presented a particle-based approach for modeling non-Fickian (anoma-
333 lous) transport in heterogeneous environments. The approach treats a par-
334 ticle trajectory as a subordinated stochastic process that is described by a
335 set of Langevin equations, which represent a CTRW at its basic level. To
336 increase the computational efficiency and accuracy of these simulations, we
337 employ the convolution-based particle tracking (CBPT) method.

338 Our analysis leads to the following major conclusions.

- 339 1. The Langevin formulation used in the CTRW-CBPT algorithm is gen-
340 eral in that no statistical restrictions are imposed on the stochastic pro-
341 cesses representing the spatial and temporal random increments. They
342 can be correlated in space and time, stationary or non-stationary, their
343 distributions are arbitrary.
- 344 2. For stationary and uncorrelated random increments, the well-known
345 partial differential equation (PDE) formulations of CTRW in terms of
346 generalized Fokker-Planck equations can be obtained by a generalized
347 Kramers-Moyal expansion.

- 348 3. The CTRW-CBPT algorithm reproduces analytical solutions for both
349 classical (ADE-based) and anomalous (a PDE formulation of CTRW)
350 transport models, with CBPT providing a significant computational
351 speed-up.
- 352 4. Finally, the CTRW-CBPT approach enables one to convert any existing
353 particle-tracking code into a simulator capable of handling non-Fickian
354 (anomalous) transport in large field-scale problems that exhibit com-
355 plex parameter structures (e.g., realistic geological settings) and com-
356 plex flow fields.

357 **Acknowledgments**

358 This research was performed under the auspices of the Los Alamos Na-
359 tional Laboratory. It was partially supported by the DOE Office of Science
360 Advanced Scientific Computing Research (ASCR) program in Applied Math-
361 ematical Sciences, and by the Office of Science (BER), Cooperative Agree-
362 ment No. DE-FC02-07ER64324. MD acknowledges the support of the EU
363 project MUSTANG, the French ANR project COLINER and CIUDEN.

364 **References**

- 365 [1] J. Bear, Dynamics of fluids in porous media, Elsevier, New York, 1972.
- 366 [2] D. Stein, F. H. J. van der Heyden, W. J. A. Koopmans, C. Dekker,
367 Pressure-driven transport of confined DNA polymers in fluidic channels,
368 Proc. Natl. Acad. Sci. 103 (43) (2006) 15853–15858.
- 369 [3] S. Koennings, J. Tessmar, T. Blunk, A. Göpferich, Confocal microscopy
370 for the elucidation of mass transport mechanisms involved in protein
371 release from lipid-based matrices, Pharmaceut. Res. 24 (7) (2007) 1325–
372 1335. doi:10.1007/s11095-007-9258-8.
- 373 [4] F. J. Rueda, S. G. Schladow, J. F. Clark, Mechanisms of contaminant
374 transport in a multi-basin lake, Ecol. Appl. 18 (8) (2008) A72–A88.
- 375 [5] L. W. Gelhar, Perspectives on field-scale application of stochastic sub-
376 surface hydrology, in: G. Dagan, S. P. Neuman (Eds.), Subsurface Flow
377 and Transport: A Stochastic Approach, Cambridge Univ. Press., New
378 York, 1997, pp. 157–176.

- 379 [6] S. P. Neuman, Adaptive Eulerian-Lagrangian finite element method for
380 advection-dispersion, *Int. J. Num. Meth. Engrg.* 20 (2) (1984) 321–337.
- 381 [7] A. Younes, M. Fahs, P. Ackerer, A new approach to avoid excessive nu-
382 merical diffusion in Eulerian-Lagrangian methods, *Comm. Num. Meth.*
383 *Engrg.* 24 (11) (2008) 897–910.
- 384 [8] E. R. Ewing, H. Wang, A summary of numerical methods for time-
385 dependent advection-dominated partial differential equations, *J. Comp.*
386 *Appl. Math.* 128 (1-2) (2001) 423–445.
- 387 [9] G. Seisenberger, M. U. Ried, T. Endress, H. Buning, M. Hallek,
388 C. Brauchle, Real-time single-molecule imaging of the infection path-
389 way of an adeno-associated virus, *Science* 94(5548) (2001) 1929–1932.
- 390 [10] A. Cortis, B. Berkowitz, Anomalous transport in “classical” soil and
391 sand columns, *Soil Sci. Soc. Am. J.* 68 (5) (2004) 1539–1548.
- 392 [11] I. M. Tolic-Norrelykke, E.-L. Munteanu, G. Thon, L. Oddershede,
393 K. Berg-Sorensen, Anomalous diffusion in living yeast cells, *Phys. Rev.*
394 *Lett.* 93 (7) (2004) 078102–1 – 078102–4.
- 395 [12] Y. Zhang, D. A. Benson, Lagrangian simulation of multidimensional
396 anomalous transport at the MADE site, *Geophys. Res. Lett.* 35 (2008)
397 L07403. doi:10.1029/2008GL033222.
- 398 [13] B. Berkowitz, H. Scher, Theory of anomalous chemical transport in frac-
399 ture networks, *Phys. Rev. E* 57 (5) (1998) 5858–5869.
- 400 [14] J. H. Cushman, M. Moroni, Statistical mechanics with three-dimensional
401 particle tracking velocimetry in the study of anomalous dispersion. I.
402 Theory, *Phys. Fluids* 13 (1) (2001) 75–80.
- 403 [15] P. Salamon, D. Fernández-García, J. J. Gómez-Hernández, Modeling
404 tracer transport at the MADE site: The importance of heterogeneity,
405 *Water Resour. Res.* 43 (2007) W08404.
- 406 [16] E. Morales-Casique, S. P. Neuman, A. Guadagnini, Nonlocal and lo-
407 calized analyses of nonreactive solute transport in bounded randomly
408 heterogeneous porous media: Theoretical framework, *Adv. Water Re-*
409 *sour.* 29 (8) (2006) 1238–1255.

- 410 [17] M. Dentz, D. M. Tartakovsky, Self-consistent four-point closure for
411 transport in steady random flows, *Phys. Rev. E* 77 (6) (2008)
412 doi:10.1103/PhysRevE.77.066307.
- 413 [18] M. M. Meerschaert, D. A. Benson, B. Baumer, Multidimensional advec-
414 tion and fractional dispersion, *Phys. Rev. E* 59 (5) (1999) 5026–5028.
- 415 [19] M. M. Meerschaert, D. A. Benson, H. P. Scheffler, P. Becker-Kern, Gov-
416 erning equations and solutions of anomalous random walk limits, *Phys.*
417 *Rev. E* 66 (2001) 060102(R).
- 418 [20] J. Klafter, R. Silbey, Derivation of continuous-time random-walk equa-
419 tions, *Phys. Rev. Lett.* 44 (2) (1980) 558.
- 420 [21] M. Dentz, B. Berkowitz, Transport behavior of a passive solute in con-
421 tinuous time random walks and multirate mass transfer, *Water Resour.*
422 *Res.* 39 (5) (2003) 1111. doi:10.1029/2001WR001163.
- 423 [22] B. Berkowitz, A. Cortis, M. Dentz, H. Scher, Modeling non-Fickian
424 transport in geological formations as a continuous time random walk,
425 *Rev. Geophys.* 44 (2) (2006) RG2003.
- 426 [23] B. Berkowitz, J. Klafter, R. Metzler, H. Scher, Physical pictures of trans-
427 port in heterogeneous media: advection-dispersion, random walk and
428 fractional derivative formulations, *Water Resour. Res.* 38 (10) (2002)
429 1191, doi:10.1029/2001WR001030.
- 430 [24] A. Cortis, C. Gallo, H. Scher, B. Berkowitz, Numerical simulation of
431 non-Fickian transport in geological formations with multiple-scale het-
432 erogeneities, *Water Resour. Res.* 40 (2004) W04209.
- 433 [25] W. Kinzelbach, The random walk method in pollutant transport simu-
434 lation, in: E. Custodio, A. Gurgui, J. P. Lobo-Ferreira (Eds.), *Ground-*
435 *water Flow and Quality Modelling*, D. Reidel Publ. Co., Norwell, Mas-
436 sachusetts, 1988, pp. 227–245.
- 437 [26] P. C. Lichtner, S. Kelkar, B. A. Robinson, New form of dispersion tensor
438 for flow in axisymmetric media with implementation in particle tracking,
439 *Water Resour. Res.* 38 (8) (2002) 21–1 – 21–16.

- 440 [27] M. Dentz, H. Kinzelbach, S. Attinger, W. Kinzelbach, Numerical stud-
441 ies of the transport behavior of a passive solute in a two-dimensional
442 incompressible random flow field, *Phys. Rev. E* 67 (2003) 046306.
- 443 [28] F. Delay, P. Ackerer, C. Danquigny, Simulating solute transport in
444 porous or fractured formations using random walk particle tracking: A
445 review, *Vadose Zone J.* 4 (2005) 360–379.
- 446 [29] A. Younes, P. Ackerer, Solving the advection-diffusion equation with the
447 Eulerian-Lagrangian localized adjoint method on unstructured meshes
448 and non uniform time stepping, *J. Comp. Phys.* 208 (1) (2005) 384–402.
- 449 [30] M. Dentz, A. Cortis, H. Scher, B. Berkowitz, Time behavior of solute
450 transport in heterogeneous media: Transition from anomalous to normal
451 transport, *Adv. Water Resour.* 27 (2004) 155–173.
- 452 [31] T. Le Borgne, P. Gouze, Non-Fickian dispersion in porous media: 2.
453 Model validation from measurements at different scales, *Water Resour.*
454 *Res.* 44 (2008) W06427.
- 455 [32] M. Dentz, H. Scher., D. Holder, B. Berkowitz, Transport behavior of
456 coupled continuous-time random walks, *Phys. Rev. E* 78 (2008) 041110.
- 457 [33] Y. Edery, H. Scher, B. Berkowitz, Modeling bimolecular reactions and
458 transport in porous media, *Geophys. Res. Lett.* 36 (2009) L02407.
459 doi:10.1029/2008GL036381.
- 460 [34] Y. Zhang, D. A. Benson, M. M. Meerschaert, H.-P. Scheffler, On using
461 random walks to solve the space-fractional advection-dispersion equa-
462 tions, *J. Stat. Phys.* 123 (1) (2006) 89–110.
- 463 [35] P. Salamon, D. Fernández-Garcia, J. J. Gómez-Hernández, Modeling
464 mass transfer processes using random walk particle tracking, *Water Re-*
465 *sour. Res.* 42 (2006) W11417.
- 466 [36] D. A. Benson, M. M. Meerschaert, A simple and efficient random walk
467 solution of multi-rate mobile/immobile mass transport equations, *Adv.*
468 *Water Resour.* 32 (2009) 532–539.
- 469 [37] P. Salamon, D. Fernández-Garcia, J. J. Gómez-Hernández, A review and
470 numerical assessment of the random walk particle tracking method, *J.*
471 *Contam. Hydrol.* 87 (3-4) (2006) 277–305.

- 472 [38] B. A. Robinson, Z. V. Dash, Users Guide for the PLUMECALC Appli-
473 cation, Los Alamos National Laboratory, Los Alamos, NM (2008).
- 474 [39] H. Risken, The Fokker-Planck equation: methods of solution and appli-
475 cations, 2nd Edition, Vol. 18 of Springer Series in Synergetics, Springer
476 Berlin Heidelberg New York, Berlin, 1996.
- 477 [40] M. Ting Lee, G. A. Whitmore, Stochastic processes directed by random-
478 ized time, *J. Appl. Prob.* 30 (1993) 302–314.
- 479 [41] H. C. Fogedby, Langevin eqations for continuous time Lévy flights, *Phys.*
480 *Rev. E* 50 (1994) 1657–1660.
- 481 [42] M. Dentz, G. Srinivasan, D. M. Tartakovsky, Non-linear Langevin equa-
482 tions and Kramers-Moyal expansions for continuous time random walks,
483 *Phys. Rev. E* submitted.
- 484 [43] W. Feller, A Introduction to Probability Theory and Its Applications:
485 Volume II, John Wiley and Sons, 1971.
- 486 [44] C. Godrèche, J. M. Luck, Statistics of occupation time renewal processes,
487 *J. Stat. Phys.* 104 (2001) 489–524.
- 488 [45] H. Scher, M. Lax, Stochastic transport in a disordered solid. I. Theory,
489 *Phys. Rev. E*.
- 490 [46] B. Berkowitz, H. Scher, Exploring the nature of non-Fickian transport
491 in laboratory experiments, *Adv. Water Resour.* 32 (2009) 750–755.
- 492 [47] I. M. Sokolov, A. Blumen, J. Klafter, Dynamics of annealed systems un-
493 der external fields: CTRW and the fractional Fokker-Planck equations,
494 *Europhys. Lett.* 56 (2001) 175–180.
- 495 [48] H. S. Viswanathan, B. A. Robinson, A. J. Valocchi, I. R. Triay, A reac-
496 tive transport model of neptunium migration from the potential reposi-
497 tory at yucca mountain, *J. Hydrol.* 209 (1) (1998) 251–280.
- 498 [49] A. Kreft, A. Zuber, On the physical meaning of the dispersion equation
499 and its solutions for different initial and boundary conditions, *Chem.*
500 *Eng. Sci.* 33 (1978) 1471–1480.

- 501 [50] F. R. de Hoog, J. H. Knight, A. N. Stokes, An improved method for
502 numerical inversion of Laplace transforms, *SIAM J. Sci. Stat. Comput.*
503 3 (1982) 357–366.
- 504 [51] C. Schwab, R. A. Todor, Karhunen-loève approximation of random fields
505 by generalized fast multipole methods, *J. Comp. Phys.* 217 (1) (2006)
506 100–122.